EFFECT OF BOUNDARIES ON THE RESPONSE OF A NEURAL NETWORK

LAWRENCE SIROVICH, SCOTT E. BRODIE, AND BRUCE W. KNIGHT, *The Rockefeller University, New York 10021 and Brown University, Providence, Rhode Island 02912 U.S.A.*

ABSTRACT The effect an abrupt boundary has upon the dynamical response of a neural network is investigated. The retina of the *Limulus* eye is used as a model system for studying this effect. A theoretical technique is presented for the quantitative prediction of the manner in which this neural network responds in the vicinity of its boundary. Corresponding experimental measurements of the response to moving stimuli by single optic neurons located near retinal boundaries are presented. Theory and experiment show detailed quantitative agreement.

INTRODUCTION

The manner in which a neuron within a functioning neural network processes information is necessarily modified by the proximity of that neuron to the network's boundary. Boundary effects may be predicted in quantitative detail by the theoretical procedure we will present below. Our procedure will be applied to a particularly well-characterized neural network, the retina of the horseshoe crab *Limulus*. A direct comparison with experimental results will be made to verify that the theory accurately predicts the way the functioning network's edge modifies the dynamical response of a retinal neuron.

In both qualitative and quantitative treatments of neural networks, it is frequently useful to assume that the network under discussion shows only slow departures from homogeneity. In other words, each portion of the network is presumed to closely resemble all comparable portions of the network with which it is in communication. This principle of neural organization provides a possible mechanism for the parallel processing that allows the nervous system to extract useful information from the ensemble of signals available to it. The basic homogeneity of several neural networks has been well established in numerous anatomical and physiological investigations.

Nonetheless, all neural networks must have boundaries, and at these boundaries, the assumption of homogeneity is no longer valid. Examples of homogeneous neural networks with boundaries occur frequently. In the visual system of mammals, each layer of the lateral geniculate nucleus constitutes such a network, as does the primary visual cortex. On a smaller scale, the so-called "columnar" organization of the cortex into bands of cells specific for ocular dominance and preferred orientation divides the cortex into an elaborate pattern of neighboring regions, separated by boundaries across which nearby cells differ greatly in functional properties. It is thus of general interest to investigate the behavior of a neural network at its boundary.

In the present investigation we consider this problem for the particular case of the lateral eye of the horseshoe crab *Limulus*, for which the assumption of homogeneity has already

proven an accurate and useful approximation. Our current knowledge of the physiology and response dynamics of the *Limulus* retina is sufficiently detailed to permit theoretical prediction of its response to arbitrary spatio-temporal illumination patterns. This theoretical description is based on the Hartline-Ratliff model (Hartline and Ratliff, 1957). Thus far, experiments have focused on the response in the central portions of the retina where, to good approximation, the neural network is homogeneous. The agreement between such experiments and predictions derived from the Hartline-Ratliff model is, in general, very good (Brodie et al., 1978*a, b*). Typical results for such studies are shown in Figs. 1 and 2.

In our experiments a retinal boundary is simulated by an edge illumination pattern. Specifically, one half of the retina is illuminated by a pattern varying in space and time; the

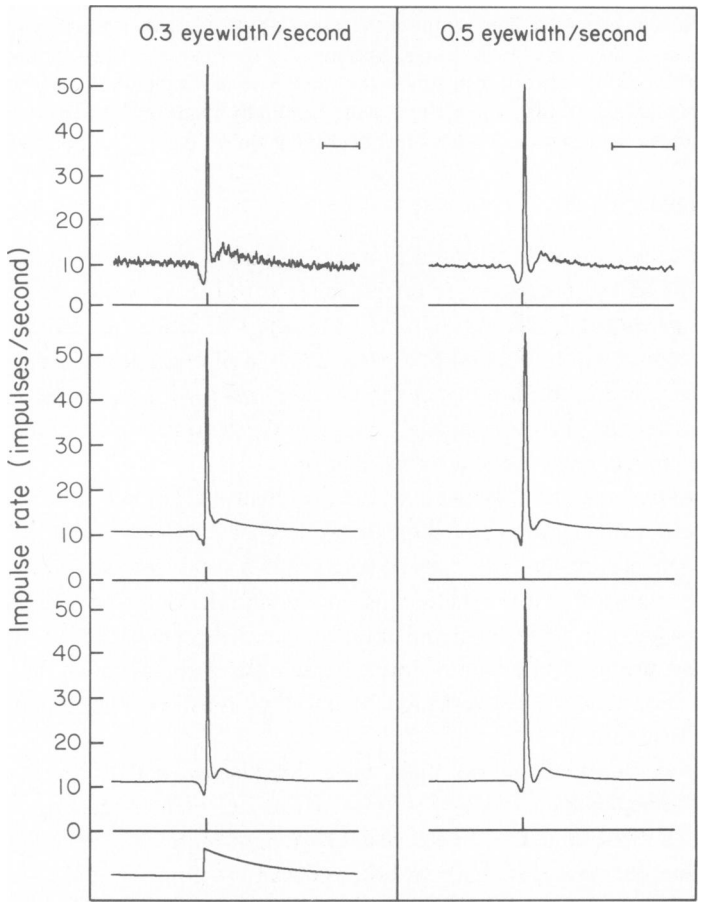

FIGURE 1 Responses to moving stimuli: comparison of responses predicted from empirical and model transfer functions. A step stimulus with exponential decay (shown at lower left) was moved across the eye at the velocities shown. The mean individual impulse rate produced by a centrally located ommatidium in response to this stimulus is shown in the top records. The middle records show the response to this stimulus predicted on the basis of the spatiotemporal transfer function measured for this ommatidium (Fig. 2, left). The bottom records show the predicted response calculated from the corresponding Hartline-Ratliff model transfer function (Fig. 2, right) Scale markers indicate 2.0 s; short vertical tick marks above the horizontal axes indicate the arrival of the stimulus step at the test ommatidium.

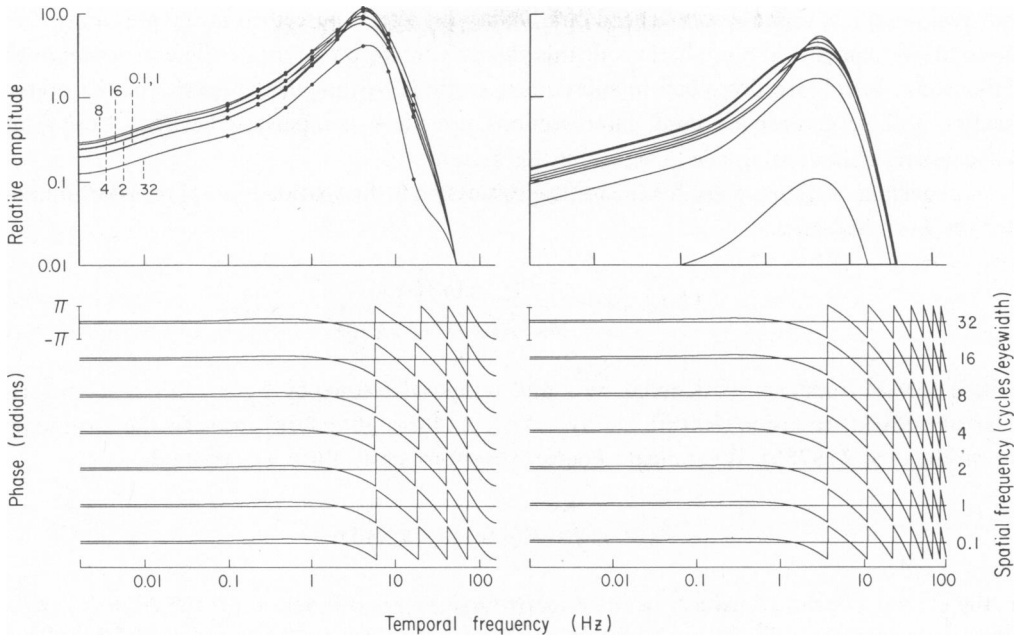

FIGURE 2 Empirical and model transfer functions. Left: Empirical spatio-temporal transfer function for the ommatidium of Fig. 1. The dots indicate measured amplitude values. Spatial frequencies (in cycles/eye width) are indicated at left; near the peak (~4 Hz) the amplitudes decrease monotonically with increasing spatial frequency. Phases are shown on separate axes for each spatial frequency, modulo 2π. Spatial frequency increases from bottom to top as indicated at right. Right: Hartline-Ratliff model transfer function with parameters chosen to match the transfer function at left. (For parameters, see Table II.) Near the peak, amplitudes decrease monotonically with increasing spatial frequency.

remaining half, on the other side of a vertical line, is held in darkness. The portion in the dark produces no neural activity and thus does not communicate with the illuminated half of the retina, as if it had been cut away by a razor. On the other hand, illumination of the full eye allows the measurement of responses which furnish a quantitative Hartline-Ratliff model for use in the edge situation. Thus the edge experiment can be placed in the same theoretical framework as the full-eye experiment, and as in Brodie et al. (1978*a, b*) we are led to the use of techniques drawn from linear signal analysis and transform theory. The termination of our homogeneous system by an abrupt boundary suggests a treatment based on the classical procedure of Wiener and Hopf (1931). This technique enables us to give a complete analytic description of the behavior of the system in the presence of an edge (also see Sirovich, 1980).

Implicit in our study is the working hypothesis that the neural organization at a boundary is, in a sense to be described later, a truncated form of that found in the interior of the retina. Support for this hypothesis comes from comparison of responses recorded near simulated boundaries with responses obtained from neurons near the actual boundary of the eye.

THEORY

The purposes of this investigation are twofold. First, our theoretical goal is to obtain an analytical procedure that yields quantitative predictions of the manner in which a neural

network responds in the neighborhood of a boundary. This is described in the present section. Second, we compare the predictions of this theory with response measurements made in the laboratory, which are described in subsequent sections. Although the results of the present section will be extensively used, later sections provide a comparison between theory and experiment without reference to details of this section.

A convenient starting point for theoretical discussion is the spatiotemporal transfer function for the *Limulus* retina:

$$F(\xi, \omega) = \frac{\tilde{P}(\xi)\tilde{E}(\omega)\tilde{G}(\omega)}{1 + \tilde{E}(\omega)\tilde{T}_L(\omega)\tilde{K}(\xi)}, \tag{1}$$

where spatial frequency is denoted by ξ and temporal frequency by ω. This embodies the Hartline-Ratliff equation (Ratliff, 1974) and except for slight modifications is the form found in Brodie et al. (1978*b*). We indicate Fourier transforms by a tilda. For example,

$$\tilde{P}(\xi) = \int_{-\infty}^{\infty} P(x)\exp(-i\xi x)\mathrm{d}x$$

is the spatial Fourier transform of the effective point spread function for the *Limulus* optics and similarly $\tilde{K}(\xi)$ is the spatial Fourier transform of the lateral inhibitory kernel $K(x)$. $\tilde{G}(\omega)$, $\tilde{E}(\omega)$, and $\tilde{T}_L(\omega)$ are the temporal transforms for the dynamics of the light to generator potential, the impulse encoder, and the lateral inhibitory process, respectively (Table I). For

TABLE I
SUMMARY OF EQUATIONS FOR HARTLINE-RATLIFF MODEL

Description	Equation
Spatiotemporal transfer function	$F(\xi,\omega) = \dfrac{\tilde{P}(\xi)\tilde{E}(\omega)\tilde{G}(\omega)}{1 + \tilde{E}(\omega)\tilde{T}_L(\omega)\tilde{K}(\xi)}$
Generator potential	$G(\omega) = e^{-i\omega t_0} \cdot \left(\dfrac{1}{1 + it_a\omega}\right)^{n_a} \cdot \left(\dfrac{1}{1 + it_b\omega}\right)^{n_b} \cdot \left(1 - \dfrac{R}{1 + it_a\omega}\right) \cdot \left(\dfrac{it_a\omega}{1 + it_a\omega}\right)^{p}$
Encoder	$\tilde{E}(\omega) = \dfrac{1}{1 + \dfrac{\kappa}{1 + i\tau\omega}} = 1 - \dfrac{\kappa/(1+\kappa)}{1 + i\dfrac{\tau}{1+\kappa}\omega}$
Lateral inhibition	$\tilde{T}_L(\omega) = \dfrac{1}{1 - C}\left[\dfrac{1}{1 + i\tau_1\omega} \cdot \dfrac{1}{1 + i\tau_2\omega} - \dfrac{C}{1 + i\tau_3\omega}\right] \cdot \dfrac{1}{1 + i\tau_4\omega}$
Fourier transform of inhibitory kernel: quotient of polynomials	$\tilde{K}(\xi) = \mathbf{K} \cdot \dfrac{1 - \left(\dfrac{\xi^2}{a^2}\right)}{\left(\dfrac{\xi}{b}\right)^4 + 2\left(\dfrac{\xi}{c}\right)^2 + 1}$
Difference of Gaussians	$\tilde{K}(\xi) = \dfrac{\mathbf{K}}{Ax_a - Bx_b}\left[Ax_a \exp(-\xi^2 x_a^2/4) - Bx_b \exp(-\xi^2 x_b^2/4)\right]$
Point spread	$\tilde{P}(\xi) = e^{-\xi^2 s^2/4}$

inversion, we write:

$$G(t) = \frac{1}{2\pi}\int_{-\infty}^{\infty} \tilde{G}(\omega)\exp(i\omega t)\mathrm{d}\omega.$$

If an illumination pattern is represented by $\mathrm{i}(x, t)$ then the transfer function (Eq. 1), can be regarded as arising from the solution by transform methods of the Hartline-Ratliff equation:

$$r(x, t) = E * (G * P * \mathrm{i} - T_L * K * r). \tag{2}$$

An asterisk in Eq. 2 indicates either a spatial or a temporal convolution product.

It is convenient to reduce Eq. 2 by means of the following definitions:

$$e = E * G * P * \mathrm{i}, \quad S = E * T_L. \tag{3}$$

In effect, e is the output of a photoreceptor in the absence of lateral inhibition: $P * \mathrm{i}$ represents the effective illumination reaching the retina after passage through the optics; G represents the transduction of this effective illumination to the intracellular generator potential; finally, E represents the transduction which encodes the generator potential into optic nerve impulses. S represents the lateral inhibitory transduction followed by the encoder. In this case Eq. 2 becomes

$$r(x, t) = e - S*K*r = e(x, t) - \int_{-\infty}^{t} S(t - t')\int_{-\infty}^{\infty} K(x - x')r(x', t')\,\mathrm{d}x'\mathrm{d}t', \tag{4}$$

and the transfer function now is

$$\mathcal{G}(\xi, \omega) = \frac{1}{1 + \tilde{S}(\omega)\tilde{K}(\xi)}. \tag{5}$$

Thus Eq. 5 relates $e(\xi, \omega)$ as input and $r(\xi, \omega)$ as output, whereas Eq. 1 relates $\mathrm{i}(\xi, \omega)$ as input and $r(\xi, \omega)$ as output.

The structures of the various transductions that occur in Eq. 1 have been discussed at length in Brodie et al. (1978*b*). With the exception of the inhibitory kernel, $K(x)$, we employ the same forms given there. For reference, these are repeated in Table I.

Inhibitory Kernel

In a previous treatment (Brodie et al., 1978*b*), $K(x)$ is represented by a difference of Gaussians. Although such a form conveniently represents the results of a number of studies (Barlow, 1967; Johnston and Wachtel, 1976; Brodie et al., 1978*b*), there is no compelling reason for this choice. Another choice, which is more conveneint for present purposes, is to represent K by a sum of decaying exponentials. Equivalent to this is the approximation of $\tilde{K}(\xi)$ (which is a directly measured quantity) by a quotient of polynomials:

$$\tilde{K}(\xi) = \frac{N(\xi^2)}{D(\xi^2)}. \tag{6}$$

Since $K(x)$ is an even function ($K(-x) = K(x)$), both polynomials must be even, as is indicated in Eq. 6. On the basis of comparison with experimental data (see Materials and Methods) we have obtained the form:

$$\frac{\tilde{K}(\xi)}{\mathbf{K}} = \frac{1 - \left(\frac{\xi}{a}\right)^2}{\left(\frac{\xi}{b}\right)^4 + 2\left(\frac{\xi}{c}\right)^2 + 1}, \tag{7}$$

where $\mathbf{K} = \tilde{K}(\xi = 0)$, and a, b, c are constants (Table II).

To recover the inhibitory kernel $K(x)$, we factor the denominator of Eq. 7:

$$\left(\frac{\xi}{b}\right)^4 + 2\left(\frac{\xi}{c}\right)^2 + 1 = \frac{(\xi^2 - \xi_1^2)(\xi^2 - \xi_2^2)}{b^4},$$

where

$$\xi_{1,2} = b\left(-\frac{b^2}{c^2} \pm \sqrt{\frac{b^4}{c^4} - 1}\right)^{1/2}, \tag{8}$$

and by convention, both ξ_1 and ξ_2 have positive imaginary parts. Then Fourier inversion of $\tilde{K}(\xi)$ gives:

$$K(x) = i\left(\frac{N(\xi_1^2)\exp(i\xi_1|x|)}{\frac{d}{d\xi}D(\xi_1^2)} + \frac{N(\xi_2^2)\exp(i\xi_2|x|)}{\frac{d}{d\xi}D(\xi_2^2)}\right). \tag{9}$$

Note that in the form of Eq. 9, ξ_1 and ξ_2 can be complex (if $b < c$) and as a result a damped sinusoidal variation is possible. Fig. 3 contains plots of $\tilde{K}(\xi)$ and $K(x)$ corresponding to the preparation of Figs. 1 and 2.

TABLE II
PARAMETERS FOR HARTLINE-RATLIFF MODEL

Parameter	Dimension	Preparation of Figs. 1–3,5–7, and 11	Preparation of Fig. 8	Preparation of Figs. 9 and 10*
t_l	seconds	0.038	0.023	0.038
t_d	seconds	0.0076	0.0061	0.0076
n_d		3	4	3
t_b	seconds	0.017	0.016	0.017
n_b		3	4	3
R		0.75	0.75	0.75
t_a	seconds	0.030	0.030	0.030
p		0.25	0.25	0.25
κ		1.5	1.0	0.5
τ	seconds	0.40	0.20	0.40
τ_1	seconds	0.036	0.030	0.050
τ_2	seconds	0.055	0.045	0.07
τ_3	seconds	0.036	0.030	0.05
τ_4	seconds	0.019	0.015	0.03
C		0.1	0.1	0.1
$\mathbf{K}$		1.0	1.5	4.0
a	Rad/eye width	17.56	21.59	23.23
b	Rad/eye width	23.61	21.58	21.66
c	Rad/eye width	24.83	14.81	27.62
A		1.5	2.0	1.2
x_a	Eye widths	0.125	0.17	0.12
B		1.65	1.2	0.75
x_b	Eye widths	0.03	0.025	0.03
s	Eye widths	0.00951	0.00653	0.00951

*Parameter set determined by comparison of observed and predicted responses to moving patterns, starting from parameter set for preparation of Figs. 1–3, etc. See text.

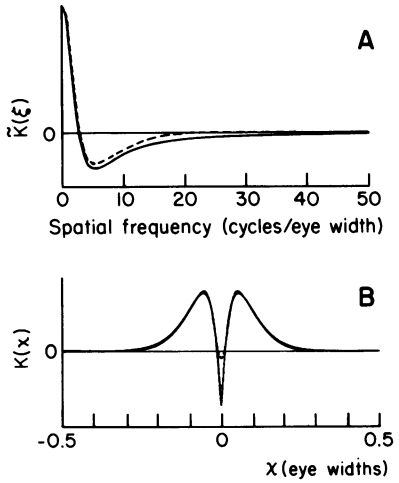

FIGURE 3 Comparison of model inhibitory kernels. Inhibitory kernels with parameters determined to match the transfer function of Fig. 2 (see Table II) are shown in the frequency domain (A) and spatial domain (B). Solid curves indicate quotient-of-polynomials kernels (Eq. 7); dashed curves indicate corresponding difference-of-Gaussian kernels (see Table I). The small disparity between the frequency-domain kernels in A corresponds to the singularity at the origin in the quotient-of-polynomials kernel in B, and is of no physiological significance.

When Eq. 7 is substituted into the transfer function, Eq. 5, we obtain:

$$\mathcal{G} = \frac{(\xi/b)^4 + 2(\xi/c)^2 + 1}{(\xi/b)^4 + 2(\xi/c)^2 + 1 + \mathbf{K}S(\omega)[1 - (\xi/a)^2]} = \frac{(\xi^2 - \xi_1^2)(\xi^2 - \xi_2^2)}{[\xi^2 - \lambda_1^2(\omega)][\xi^2 - \lambda_2^2(\omega)]}, \tag{10}$$

where

$$\lambda_{1,2} = b\left\{\left(\frac{\mathbf{K}S(\omega)b^2}{2a^2} - \frac{b^2}{c^2}\right) \pm \left[\left(\frac{b^2}{c^2} - \frac{\mathbf{K}S(\omega)b^2}{2a^2}\right)^2 - (1 + \mathbf{K}S(\omega))\right]^{1/2}\right\}^{1/2}. \tag{11}$$

The square roots in Eq. 11 are chosen so that λ_1, λ_2 have positive imagainary parts.

Uniformly Drifting Pattern

The case considered in Brodie et al. (1978*a*) was that of a drifting pattern moving across the full eye with uniform speed. In the present context this means a stimulus of the form

$$e = e(x + Vt),$$

where V is the speed of movement (measured in eyewidths/s). The solution to Eq. 4 with this form of e is easily obtained by transform methods:

$$r(x + Vt) = \frac{1}{2\pi}\int_{-\infty}^{\infty} \frac{\tilde{e}(\xi)\exp[i\xi(x + Vt)]}{1 + S(\xi V)\tilde{K}(\xi)}\,d\xi.$$

An alternate form, useful in later discussion, is

$$r(x + Vt) = \frac{1}{2\pi}\int_{-\infty}^{\infty} \frac{\exp\left[i\omega\left(t + \frac{x}{V}\right)\right]}{1 + S(\omega)\tilde{K}\left(\frac{\omega}{V}\right)}\left[\frac{1}{|V|}\tilde{e}\left(\frac{\omega}{V}\right)\right] d\omega$$

$$= p_f * e(Vt), \tag{12}$$

where $e(Vt)$ is simply $e(x + Vt)$ evaluated at the origin, and

$$p_f = \frac{1}{2\pi}\int_{-\infty}^{\infty} \mathcal{G}\left(\frac{\omega}{V}, \omega\right) \exp\left[i\omega\left(t + \frac{x}{V}\right)\right] d\omega. \tag{13}$$

We use the subscript f to indicate that the full eye (in our idealization, infinite) is being described.

p_f is the solution for a moving delta function stimulus $e = \delta(x + Vt)$, and is referred to as the solution operator. It does not depend on any particular illumination pattern. However, as indicated in Eq. 12, it may be used to construct the solution for an arbitrary stimulus pattern.

For future reference we note:

$$\tilde{p}_f(x = 0, \omega) = \tilde{p}_f(0, \omega) = \mathcal{G}\left(\frac{\omega}{V}, \omega\right) = \frac{\left(\frac{\omega^2}{V^2} - \xi_1^2\right)\left(\frac{\omega^2}{V^2} - \xi_2^2\right)}{\left[\frac{\omega^2}{V^2} - \lambda_1^2(\omega)\right]\left[\frac{\omega^2}{V^2} - \lambda_2^2(\omega)\right]}, \tag{14}$$

where Eq. 8 has been substituted, and in this same vein,

$$\tilde{p}_f(x, \omega) = \tilde{p}_f(0, \omega) \exp\left(\frac{i\omega x}{V}\right). \tag{15}$$

Response at a Boundary

The main problem considered in this paper concerns the response experienced at the boundary of an eye. A related problem is that of the response at a shadow edge. In this case the eye is separated by a straight line into two portions: one portion, say that on the right, is illuminated; the other is kept entirely in the dark. This simulation of the natural boundary is the case treated in most of our experiments.

For the situation just depicted, the ommatidia to the left of the edge, $x < 0$, do not respond and hence do not affect those to the right, $x > 0$. Therefore, instead of Eq. 4, the Hartline-Ratliff equation now becomes:

$$r(x, t) = e(x + Vt) - \int_{-\infty}^{t} S(t - t') \int_{0}^{\infty} K(x - x')r(x', t')\, dx'dt'. \tag{16}$$

Unlike the full-eye problem, Eq. 16 cannot be solved by direct application of Fourier transform methods. At the root of the difficulty is the fact that $r(x, t)$ is defined only for $x \geq 0$, whereas the integral term of the right-hand side is also defined for $x < 0$. We may thus define:

$$-q(x, t) = e(x + Vt) - \int_{-\infty}^{t} S(t - t') \int_{0}^{\infty} K(x - x')r(x', t')\, dx'dt', \; x < 0.$$

The new variable, q, is unknown as long as $r(x, t)$ is unknown. If we now set $r(x, t) = 0$ for $x < 0$ amd $q(x, t) = 0$ for $x > 0$, then Eq. 16 can be written as:

$$r = e + q - S * K * r, \quad -\infty < x < \infty.$$

The convolution term now factors under Fourier transformation, but we are then left with one equation in the two unknowns $\tilde{r}$ and $\tilde{q}$. If we consider the definition of the Fourier transform, for example,

$$\tilde{r}(\xi) = \int_{-\infty}^{\infty} r(x) \exp(-i\xi x)\, dx = \int_{0}^{\infty} r(x) \exp(-i\xi x)\, dx,$$

we see that as a result of their definitions, $\tilde{r}(\xi)$ is analytic in the lower half, and $\tilde{q}(\xi)$ is analytic in the upper half, of the complex ξ-plane. This fact leads to solution of the edge problem, by means of a classical method due to Wiener and Hopf (1931) (also see Noble, 1958). The actual method of solution is too lengthy to be given here. A complete analysis is given in Sirovich (1980).

Fortunately, the representation of the solution to Eq. 16 is relatively simple, notwithstanding its lengthy derivation. It is convenient to introduce the solution operator to Eq. 16 by writing

$$r = p_e * e,$$

where the subscript e indicates that the edge solution is being considered. Then the transform of the solution at the edge itself is given by:

$$\tilde{p}_e(0, \omega) = \frac{\left(\frac{\omega}{V} + \xi_1\right)\left(\frac{\omega}{V} + \xi_2\right)}{\left(\frac{\omega}{V} + \lambda_1\right)\left(\frac{\omega}{V} + \lambda_2\right)} = \frac{\left(\frac{\omega}{V} - \lambda_1\right)\left(\frac{\omega}{V} - \lambda_2\right)}{\left(\frac{\omega}{V} - \xi_1\right)\left(\frac{\omega}{V} + \xi_2\right)} p_f(0, \omega), \tag{17}$$

whereas for $x > 0$

$$\begin{aligned}\tilde{p}_e(x, \omega) = \tilde{p}_f(0, \omega) &\left\{\exp\left(\frac{i\omega x}{V}\right) - \frac{1}{2}\left[\exp(i\lambda_1 x) + \exp(i\lambda_2 x)\right]\right\} \\ &+ p_e(0, \omega)\left[\frac{\exp(i\lambda_1 x) + \exp(i\lambda_2 x)}{2}\right. \\ &\left. + \frac{\exp(i\lambda_1 x) - \exp(i\lambda_2 x)}{(\lambda_1 - \lambda_2)}\left(\frac{(\lambda_2 - \xi_1)(\lambda_2 - \xi_2)}{\lambda_2 - \frac{\omega}{V}} + \frac{(\lambda_1 - \xi_2)(\lambda_1 - \xi_1)}{\lambda_1 - \frac{\omega}{V}}\right)\right].\end{aligned} \tag{18}$$

Several features of Eqs. 17 and 18 merit comment. Comparison of Eq. 17 with the comparable full eye result Eq. 14, indicates that it represents in a special way half of the factors of p_f. In fact, since λ_1, λ_2 have positive imaginary parts we see from the first form of Eq. 17 that the denominator does not vanish for $V < 0$ when ω lies in the lower half plane, and it may be further shown to contain no other singularities. Hence $p_e(0, \omega)$ represents a causal expression for $V < 0$. This should be since a stimulus arriving at the edge from the dark side ($V < 0$) elicits no response before its arrival. When $V < 0$, the expression in Eq. 17 is no longer

causal, which signals the fact that an anticipatory "Mach band" should then appear. We also note that at $x = 0$, Eq. 18 reduces to Eq. 17. Furthermore, because λ_1 and λ_2 have positive imaginary parts, we recover the full-eye result (Eq. 15) when $x \rightarrow \infty$ in Eq. 18.

An arbitrary moving illumination pattern, $e(x + Vt)$, has, at the origin, the temporal transform,

$$\tilde{e}_0(\omega) = \frac{1}{|V|}\tilde{e}\left(\frac{\omega}{V}\right).$$

The solution to the simulated boundary problem is therefore given by:

$$r(x, t) = \frac{1}{2\pi}\int_{-\infty}^{\infty} \tilde{e}_0(\omega)\, \tilde{p}_e(x, \omega) \exp(i\omega t)\, d\omega. \tag{19}$$

To complete the analysis we return to Eq. 2 and its solution. This is easily accomplished by transforming Eq. 3, which yields:

$$\tilde{e}_0(\omega) = \tilde{E}(\omega)\tilde{G}(\omega)\tilde{P}\left(\frac{\omega}{V}\right)\tilde{i}_0(\omega), \tag{20}$$

where $\tilde{i}_0(\omega)$ is the temporal transform of $i(x + Vt)$ at $x = 0$. The full solution is therefore given by the substitution of Eq. 20 into Eq. 19. In view of the complicated form of the various transductions (see Table I) no explicit representation in terms of well-known functions can be expected to result from Eq. 19 with Eq. 20 substituted. (For a special case where explicit forms occur, see Sirovich, 1979.) As a result Eq 19 is evaluated by discrete methods for which the Fast Fourier Transform (FFT) algorithm can be used.

MATERIALS AND METHODS

The experimental methods employed in this study were essentially those of Brodie et al. (1978*a*). A few changes in procedure are noted below.

Time-varying stimulus patterns were produced on a display oscilloscope under computer control and conveyed to the *Limulus* eye by lens and a fiber-optic taper. As a rule, two types of stimuli were presented in alternation: "analysis stimuli," which consisted of counter-phase modulated sinusoidal gratings, and "synthesis stimuli," in which spatial patterns moving at constant velocity were presented to the eye to generate responses for comparison with the theoretical predictions. For all stimuli, the frame rate was 39.1 Hz, and the spatial resolution was 256 points/eye width. For some episodes, a computer-generated blanking signal was used to darken one half of the display screen to generate edge illumination of the test ommatidium. This edge was placed ~0.05 eye widths away from the nominal position of the test ommatidium, to ensure its full illumination, despite the finite point-spread characteristic of the stimulus optics and small uncertainties in the alignment of the stimulus with the test ommatidium.

Adult male horseshoe crabs, *Limulus*, measuring 15–20 cm across the carapace were obtained from Gulf Specimens, Inc., Panacea, Fla. Optic nerve activity was monitored using an *in situ* preparation (Biederman-Thorson and Thorson, 1971; Kaplan and Barlow, 1975). The optic nerve was cut and introduced into a chamber mounted in the carapace. The nerve was dissected with glass needles until a fiber containing a single functioning axon was obtained. Cotton wick-silver/silver chloride electrodes were used for recording. The temperature of the crab was held at 22 ± .25°C by means of a constant-temperature circulator coupled to the animal through a modified ice bag (Brodie, 1979). This elevated temperature was chosen because it raises the mean impulse rate (Adolph, 1973) and enhances the response to flickering light (Brodie, 1979). Nerve impulse times were recorded by computer, with a resolution of 10^{-4} s.

To preserve the eye's state of light adaptation, the experiments consisted of 60-s periods of illumination in alternation with 90-s periods of darkness. For those experiments performed on test ommatidia near the center of the eye, episodes alternated between analysis stimuli and synthesis stimuli. The successive analysis episodes passed in turn through each of eight spatial frequencies. Successive synthesis episodes presented the moving stimulus in opposite directions, first in the full-eye configuration, and then with simulated boundary illumination. Stimulus velocities of 0.3, 0.5, 0.8, and 1.3 eye widths/s were used.

One potential problem with this protocol arises because that half of the retina kept in darkness during the simulated-edge episodes receives 25% less total illumination over the duration of the experiment than does the other half, which is illuminated during every episode. In principle, this difference could induce different states of light adaptation in the two halves of the retina. As this possibility was effectively ruled out by comparison of responses to mirror-image stimuli presented in the full-eye configuration (Fig. 7, below), it was deemed unnecessary to compensate for this potential complication.

In addition to the simulated boundary experiments, we also measured the responses to moving stimuli of ommatidia as close as possible to the actual boundary of the *Limulus* eye. As our optical system often couples imperfectly to such extreme ommatidia, it was difficult to obtain adequate impulse rates from many units at the extreme periphery. In our most successful experiment of this type, we recorded from an ommatidium located 3–4 ommatidial diameters from the anterior border of the eye. This unit produced a mean impulse rate of ~7 impulses/s. For this experiment only moving pattern stimuli were used. As this ommatidium was effectively at the boundary of the eye, it was unnecessary to use a simulated edge boundary stimulus. Accordingly, in this experiment, the illumination extended well beyond the natural border of the eye, and the experimental protocol consisted of drifting patterns moving at several velocities in opposite directions across the boundary of the eye.

The full-eye moving stimuli are shown in Fig. 4 A and B, and may be expressed formally by:

$$i_f(x, t) = M + H[\mathrm{sgn}(V) \cdot (x + Vt)] \cdot \exp[-\mathrm{sgn}(V) \cdot (x + Vt)], \qquad (21)$$

where M is a stimulus intensity offset. H, the Heaviside function, is 0 for negative arguments, and 1 for

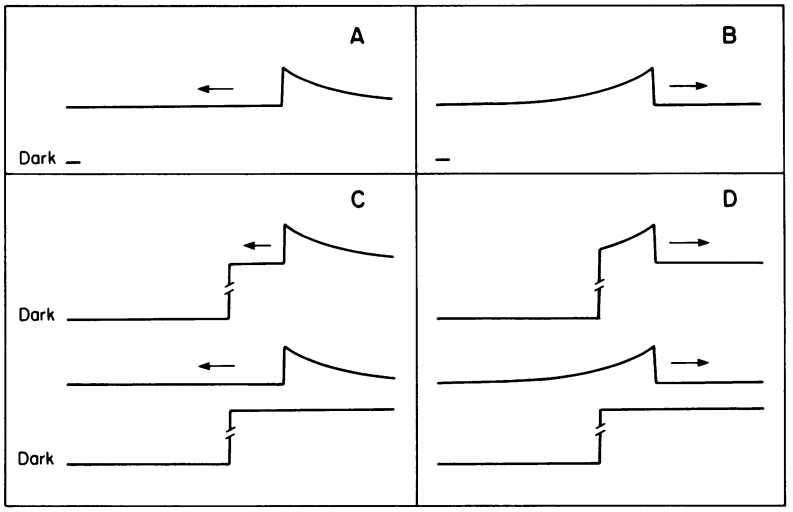

FIGURE 4 Comparison of full-eye and simulated-boundary stimuli. (A) Full-eye stimulus, moving to the left. (B) Full-eye stimulus, mirror image of A. Step moves to right. (C) Formation of edge stimulus, with step appearing out of light. Stationary step pattern, with left half of eye in darkness (bottom) is multiplied by moving stimulus as in A to produce simulated-boundary stimulus, top. (D) Formation of edge stimulus, with step appearing out of the dark. Stationary step pattern with left half of eye in darkness (bottom) (as in C) is multiplied by moving stimulus as in B to produce simulated-boundary stimulus, top.

positive arguments. The signum function, sgn(V), is 1 or -1 as V is positive or negative, respectively. The stimuli were repeated every $4/V$ s; this produced the appearance of an endless series of step-transients followed by exponential decays, with each decay 4 eye widths in length. Simulated edge stimuli were of the form

$$i_e(x, t) = H(x) \cdot i_f(x, t).$$

Thus the moving pattern either moved from the periphery of the eye toward the simulated edge ($V > 0$ in Eq. 21, Fig. 4 C), or appeared suddenly at the simulated edge and moved towards the periphery ($V < 0$ in Eq. 21, Fig. 4 D). The exponential form of these stimuli was chosen to obtain a periodic stimulus with sharp "on-transients" but without sharp "off-transients." This choice minimized the truncation of transient responses to dark stimulus features, which, as a significant nonlinearity in the *Limulus* eye, is beyond the scope of the linear analysis undertaken in this study (Brodie et al., 1978*a*).

Procedures for the measurement and extrapolation of the empirical spatiotemporal transfer function have been described in detail elsewhere (Brodie et al., 1978*a*); in brief, the transfer function value $\mathcal{F}(\xi, \omega)$ is defined as the ratio between output and input for a complex stimulus of the form $i(x, t) = \exp(i(\xi x + \omega t))$.[1] By virtue of the linearity and symmetry of the *Limulus* retina, this ratio may be determined from the harmonic content at the frequency ω_n of the response to a complex analysis stimulus of the form $i(x, t) = \cos\xi x \cdot \Sigma_n c_n \exp(i\omega_n t)$, where the c_n are chosen so that the response has roughly equal power at each stimulus frequency ω_n. The harmonic content of the neural response, in terms of the mean impulse density $r(t)$, was determined by means of a least-squares algorithm (Brodie et al., 1978*a*, Appendix B). A two dimensional cubic spline procedure was used to estimate transfer-function values at spatiotemporal frequencies between the points of the frequency lattice at which it was measured. Extrapolation to very high frequencies (in space and time) was performed so as to continue the roll-off observed at moderately high frequency. Extrapolation to low temporal frequency was based on the observations of Biedermann-Thorson and Thorson (1971) that at such frequencies, the transfer function is proportional to $(i\omega)^p$, where p ranged from 0.18 to 0.27; we used $p = 0.25$. Extrapolation to low spatial frequency was unnecessary.

Except as discussed below, our procedures for adjusting the parameters of our model for the *Limulus* spatiotemporal transfer function to fit an empirical transfer function were the same as those of Brodie et al. (1978*b*).

Our present theoretical method becomes particularly tractable if we fit the inhibitory spatial modulation transfer function, $\tilde{K}(\xi)$, not by a difference of Gaussians (as in Brodie et al. 1978*b*) but rather by a quotient of two polynominals. Our total number of measurements of $\tilde{K}(\xi)$ were consistent with a choice of the form:

$$\tilde{K}(\xi) = \frac{a_2\xi^4 + a_1\xi^2 + a_0}{b_3\xi^6 + b_2\xi^4 + b_1\xi^2 + 1}. \tag{22}$$

The experimental values, $\tilde{K}(\xi_n)$, observed at spatial frequencies ξ_n may be substituted into Eq. 22 which, for the various experimentally chosen values of ξ_n, then becomes a set of linear simultaneous equations that may be solved for the six a_i, b_i. However, it is a generic property of functions that lie close to the empirical $\tilde{K}(\xi)$ that both numerator and denominator of Eq. 22 will be endowed with spurious and almost superimposed roots if this procedure is followed. Thus the empirical form of $\tilde{K}(\xi)$ generically forces the choice of $a_2 = 0$, $b_3 = 0$ for an acceptable fit. In consequence we obtain the simpler form given by Eq. 7. Parameters for difference-of-Gaussian kernels equally compatible with experimental data were estimated for the purpose of comparison with earlier work. The two forms for $\tilde{K}(\xi)$ are compared in Fig. 3. Parameters for three *Limulus* preparations are given in Table II.

[1]Here we represent sinusoidal functions in terms of corresponding complex exponentials. For example, the expression $\exp[i(\xi x + \omega t)]$ represents the real travelling wave $\cos(\xi x + \omega t)$.

Fourier synthesis calculations were performed on arrays of 1,024 points by means of the FFT algorithm. The model transfer function for the full eye was computed from Eq. 1.

Comparison of Theoretical and Experimental Results

The recorded firing times of a neuron are converted to an instantaneous impulse rate given by the reciprocal of the time inverval between successive neural impulses. The response taken in this fashion is averaged over many records to give the mean individual rate σ. On the other hand, the theoretical calculations above predict the response in terms of the mean impulse firing density, r, of an ensemble of like encoders (Knight, 1972). At relatively high firing rates and slow modulation, r and σ approach one another. On the other hand, if both r and σ show only small time-dependent departures from a mean impulse rate, they may be related by means of a linear transduction (Brodie et al., 1978*a*). In the cases treated here, neither of these criteria are met, and a more detailed, nonlinear treatment of the

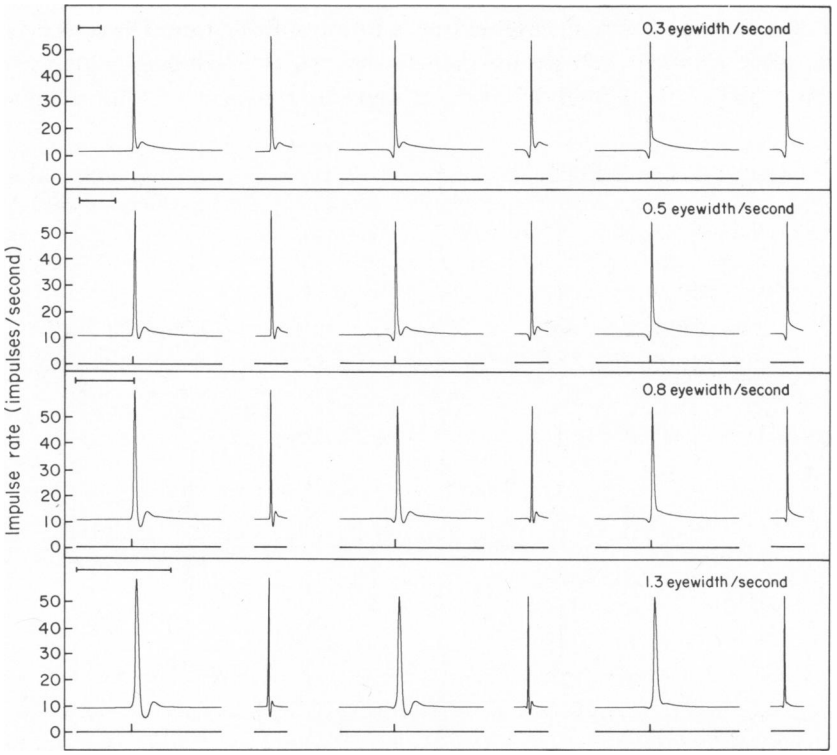

FIGURE 5 Predicted edge and full-eye responses to moving stimuli, based on the model transfer function of Fig. 2. Responses were calculated at four stimulus velocities, as shown at right. For each velocity, the two records at left show the predicted response to a simulated boundary stimulus, with the step coming out of the dark; the middle two records show the predicted response to moving steps for the full-eye stimulus; and the two records at right show the predicted response to a simulated boundary stimulus, with the step coming out of the light. The scale markers at left apply to the longer record of each pair, and represent 2.0 s. The short vertical tick marks above the horizontal axes for these records indicate the arrival of the moving step at the test ommatidium. The longer records are plotted with horizontal scales proportional to stimulus velocity, so that horizontal distance on these records represents distance on the retina at the same scale for all velocities. The shorter record of each pair depicts the response transient of the corresponding long record, replotted on a uniform time scale for all velocities. (The scale marker shown for 0.3 eye width/s also represents 2.0 s on all the short records.

transduction from r to σ is required. A brief analytical discussion of this procedure is given in the Appendix; a full treatment may be found in Knight et al. (1979).

RESULTS

The predicted responses to moving stimuli, which consist of step-transients followed by exponential decays (see Materials and Methods), are shown in Fig. 5. These records were calculated according to the theory outlined above, under the assumption that the test ommatidium is located exactly at the edge of the active neural network ($x = 0$). The waveforms show a significant dependence on the velocity of the moving step.

At low speed (0.3 eye widths/s) the full-eye response shows a prominent anticipatory Mach band (Ratliff, 1965) followed by a vigorous upstroke as the step crosses the test ommatidium. Following this on-transient, there is a rapid return to a moderate impulse rate, with a marked "notch" in the response before the eye returns to its mean firing rate. The slow decline in the mean rate after transient activity associated with the step crossing is due to both the exponential shape of the stimulus waveform and the dynamics of light adaptation. The

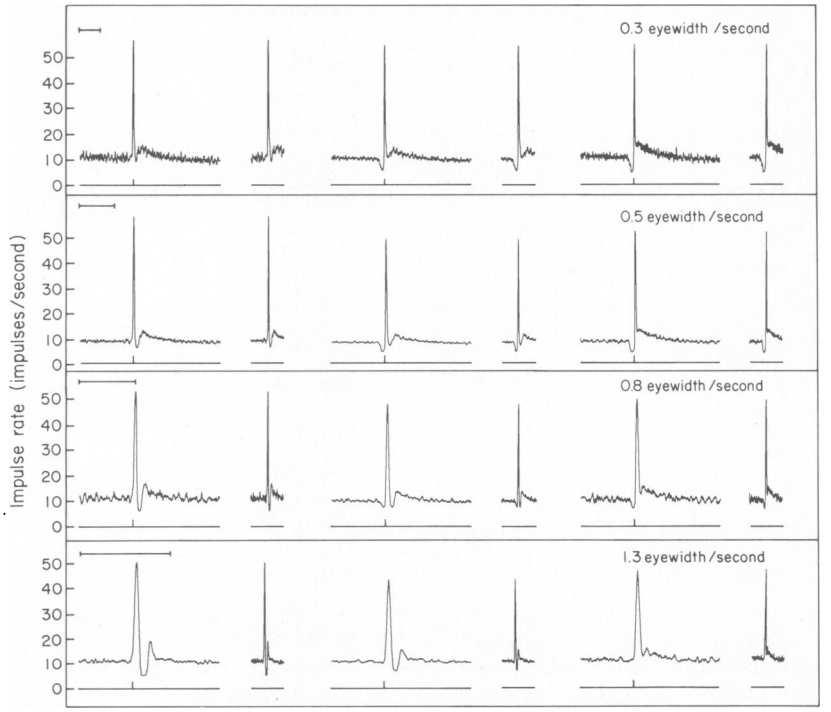

FIGURE 6 Observed edge and full-eye responses to moving stimuli. Measured responses to stimuli moving at four velocities are shown, plotted in the same manner as the predictions of Fig. 5. Responses to steps moving out of the dark are shown at left; responses to steps moving "out of the light" are shown at right. Middle column records show the average of responses to steps moving in both directions, with full-eye illumination (see Fig. 7). Each response is plotted (long records) on a uniform space scale (time scale proportional to velocity; scale markers at left represent 2.0 s); the response transients (short records) are also replotted on a uniform time scale (scale marker for 0.3 eye width/s represents 2.0 s for all short records). Short vertical tick marks indicate arrival of moving step at test ommatidium.

edge-illumination responses show marked differences from the full-eye response. When the step appears "out of the dark," there is no Mach band preceding the on-transient, but the decay following the step-crossing closely resembles that seen for the full-eye case. Conversely, when the step appears from the illuminated side of the edge ("out of the light"), there is an anticipatory Mach band similar to that seen in the full eye, but the decay following the on-transient lacks the notch seen in the full-eye response.

As the velocity is increased, two trends may be noted in the predicted response for full-eye illumination. First, the anticipatory Mach band becomes reduced in size, and second, the notch after the on-transient becomes much more prominent, as does the secondary maximum that follows it. Corresponding trends may readily be perceived in the responses under edge illumination to steps moving in the appropriate direction: out of the dark the notch following the on-transient grows, whereas out of the light the anticipatory Mach band shrinks as velocity is increased. It may also be noticed that at high velocities, a small notch appears following the transient in the out-of-the-light direction. Finally, at high velocities, the height of the on-transient for the out-of-the-dark stimulus becomes noticeably greater than that seen in either the full-eye or out-of-the-light stimulus conditions.

The responses actually observed from the ommatidium whose dynamics are predicted in Fig. 5 are shown in Fig. 6. Direct superposition of the records shows that the agreement between predicted and observed responses is in general very good, though the precision of the agreement appears to be slightly less at the highest velocities. All of the qualitative features described above for the model records may readily be seen in the actual responses. The predicted changes in the response with increasing velocity are likewise evident. Direct superposition of theory and experiment is not shown here and in what follows since for the most part theoretical curves are masked by the noise in the comparable experimental records. Similarly a numerical calculation of the fit of theory to experiment measures experimental noise more than the fit itself and is therefore not given.

It is instructive to compare these records with the responses to full-eye illumination with

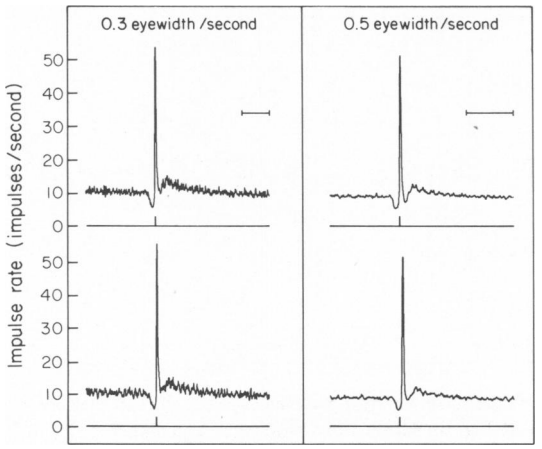

FIGURE 7 Comparison of responses to mirror-image, full-eye stimuli. Responses to steps moving in opposite directions across the full eye (see Fig. 4 A, B) are shown for two stimulus velocities. Scale markers indicate 2.0 s; vertical tick marks indicate arrival of moving step at test ommatidium.

step stimuli moving in opposite directions (Fig. 7). This serves as a control against the possibility that the retina itself is asymmetrical, or that the two portions of the eye are in a significantly different state of light adaptation. The observed similarity of responses rules out such asymmetry as a contributing factor to the effects documented in Fig. 6. We have exploited this symmetry by averaging responses to mirror-image, full-eye stimuli in all the other full-eye records depicted in this paper.

The difference between the peak height of the response to step transients moving rapidly towards or away from the simulated boundary of the neural network is clearly illustrated in data from another *Limulus* preparation (Fig. 8). For this eye, the peak response to a step coming out of the dark was ~50% greater than the response to a step coming out of the light. Similar responses have been observed whenever we have presented these simulated-edge stimuli to the *Limulus* retina.

In one experiment (see Materials and Methods) we attempted to measure the responses to moving steps of an ommatidium as near as possible to the actual boundary of the *Limulus* retina. The ommatidium selected for the experiment was within three or four ommatidial diameters (~0.1 eye widths) of the edge of the eye. (This compares with a maximum ommatidial edge displacement in the simulated edge experiments of 0.05 eye widths.) The results of this experiment are shown in Fig. 9. Though there is a slight anticipatory Mach band seen at low velocities in the response to a step which is nominally coming out of the dark (which is presumably due to the slight displacement of the ommatidium from the edge of the eye), the similarity between these records and those recorded at simulated edges in the interior of the neural network is unmistakable: steps coming out of the light show prominent anticipatory Mach bands and only small notches in the response after the peak response transient. Steps in the other direction produce little anticipation, but show a marked interval of inhibition following the peak transient response. The height of the peak response to steps coming out of the dark is greater than that of the response to steps moving in the other direction.

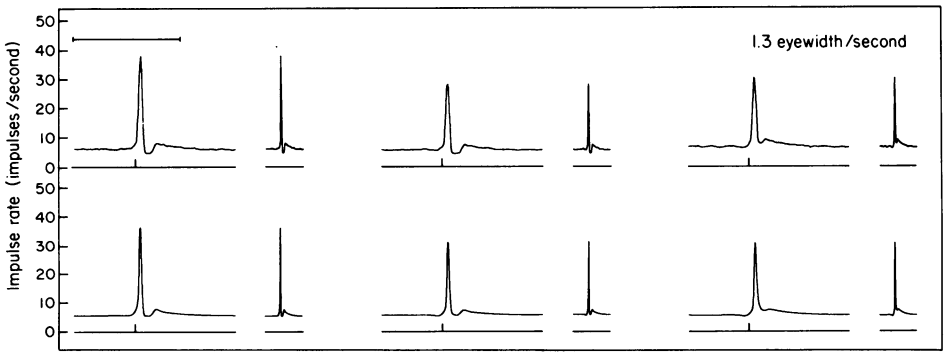

FIGURE 8 Effect of simulated boundary for high velocity stimuli. Top row: observed responses to moving step stimuli, plotted as in Fig. 6. Bottom row: predicted responses; see Table II for transfer function parameters. Records at left show response to stimuli moving out of the dark; records at right show response to stimuli moving out of the light; middle records show response to full-eye stimuli. Scale marker represents 2.0 s (long records). Short records show response transients, replotted for comparison with Fig. 6. (Short records are 3.08 s long.) Tick marks indicate arrival of moving step at test ommatidium.

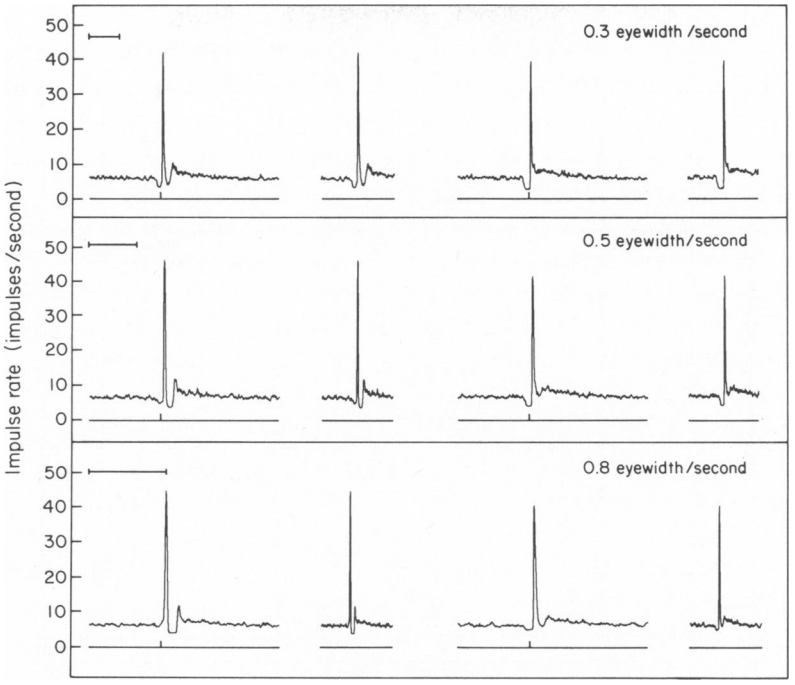

FIGURE 9 Observed responses of an ommatidium near the boundary of the eye to moving stimuli. Measured responses to stimuli moving at three velocities are shown. Responses to stimuli moving from the periphery toward the interior of the eye (analogous to stimuli moving out of the dark in simulated edge experiments) are shown at left; responses to stimuli moving from the interior of the eye toward the periphery (analagous to stimuli moving out of the light in simulated edge experiments) are shown at right. Test ommatidium was ~0.1 eye width (3–4 ommatidial diameters) from the anterior boundary of the eye. Long records are plotted on uniform space scale (time scale proportional to velocity; scale markers at left indicate 2.0 s). Short records show response transients replotted on uniform time scale (scale marker for 0.3 eye width/s indicates 2.0 s for all short records). Short vertical tick marks indicate arrival of moving step at test ommatidium.

Our procedures for the measurement of an empirical transfer function could not be applied to this edge ommatidium because of its demonstrably asymmetric inhibitory field. Thus, to assess the compatibility of the responses from this unit with the Wiener-Hopf treatment of the Hartline-Ratliff model, it was necessary to calibrate a set of model parameters by comparison of the observed responses with the predictions of model calculations, instead of by comparison of empirical and model transfer functions. The parameters for the model transfer function of Fig. 2 were used as a starting poing for the parameter search, and were modified only as dictated by specific response features. In the final parameter set (Table II), the generator potential parameters were adopted without change. Small changes were required for most of the parameters of the self- and lateral-inhibitory processes, but it was necessary to increase the total lateral inhibitory strength to several times its previous value. (The significance of this observation is discussed below.) The results of this fitting procedure are shown in Fig. 10. These calculations included provision for the finite distance between the test ommatidium and the edge of the retina (Eq. 18).

Indeed, such calculations, which allow for the small offset between the simulated boundary

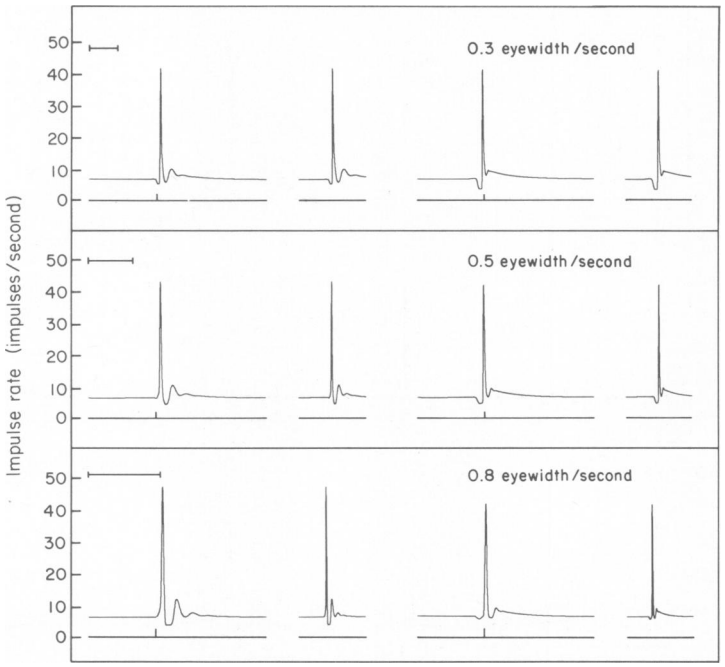

FIGURE 10 Calculated responses of ommatidium near the boundary of the eye to moving stimuli. Estimated responses calculated from model transfer function with parameters adjusted for compatibility with measured responses of Fig. 9. (See Table II for parameter values.) Records at left show calculated responses to stimuli moving from the periphery toward the interior of the eye; records at right show calculated responses to stimuli moving from the interior toward the periphery of the eye. Scale markers at left indicate 2.0 s (long records); short records show response transients replotted on uniform time scale (scale marker for 0.3 eye width/s indicates 2.0 s for all short records). Tick marks indicate arrival of moving step at test ommatidium.

and the test ommatidium (Fig. 11), also account for the small notches in the response records following the peak transient response to steps moving out of the light in the experiment of Fig. 6.

DISCUSSION

The agreement between the Wiener-Hopf calculations and the observed responses of the *Limulus* retina to simulated edge stimuli constitutes additional evidence of the adequacy of the Hartline-Ratliff model for the quantitative description of the dynamic response of the *Limulus* eye. In this paper, we extend to nearly two orders of magnitude the range of stimulus velocities over which the model appears valid. Our empirical transfer function measurements are not sufficiently accurate at temporal frequencies that considerably exceed the mean impulse rate to enable us to critically evaluate the calibration of the model at velocities much greater than those presented above. In any event, preliminary experiments and model calculations suggest to us that there are no further significant quantitative changes to be seen in the retinal response at higher velocities.

Though the calculations described above model the observed responses directly in terms of the analytical structure of the Hartline-Ratliff model, it is nonetheless useful to describe the

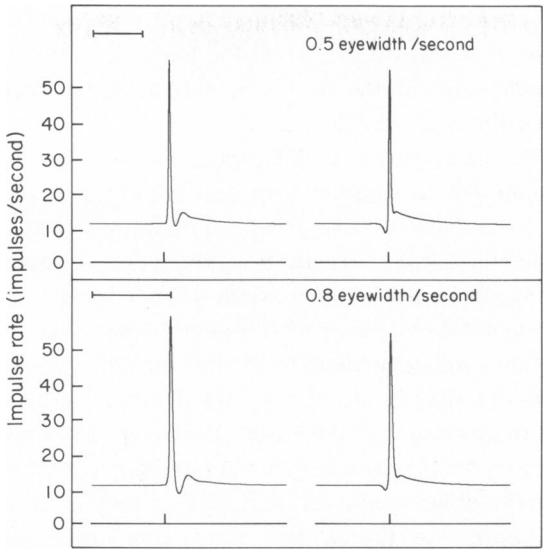

FIGURE 11 Predicted responses to moving stimuli, including small offset between simulated edge and test ommatidium; preparation of Figs. 5 and 6. Offset was 0.05 eye widths, or 2 ommatidial diameters. Records at left simulate responses to stimuli coming out of the dark, records at right for stimuli coming out of the light. Scale markers at left represent 2.0 s; tick marks indicate arrival of moving step at test ommatidium.

responses to edge stimuli in terms of the physiological processes that underly the model. The large peak response in the impulse rate results from the light-to-generator potential transduction, followed by the encoder transduction, which includes self-inhibition. As the step stimulus moves across the eye this excitatory peak is accompanied by zones of decreased neural response, as mediated by the spatial and dynamic properties of the lateral inhibitory transduction. The shape of these moving Mach bands depends on the stimulus velocity; at high speeds, the moving step tends to "overrun" the lateral inhibition, so that the anticipatory Mach band is much less pronounced than that following the excitatory transient.

The effect of the simulated edge on these response features is straightforward. In the out-of-the-light configuration, the test ommatidium shows an essentially typical full-eye response so long as it remains ahead of the advancing edge. Just after the step crosses the test ommatidium, producing the usual excitatory transient, it passes beyond the illuminated portion of the eye. The test ommatidium is thus not in a position to receive the burst of inhibitory impulses which would follow in the full-eye setting. The impulse rate therefore declines gradually, reflecting the intensity of the stimulus and the dynamics of light adaptation and self inhibition. At high speeds, the self-inhibitory process can produce a small notch in the response after the on-transient (Figs. 5 and 8). Conversely, in the out-of-the-dark configuration the test ommatidium is the first unit in the retina to be excited by the moving step. Thus, there is no anticipatory Mach band whatever. Subsequently, as the step moves away from the test ommatidium it is inhibited by the on-transient in essentially the same fashion as in the full-eye situation.

At high speeds, the height of the on-transient peak is greater for steps moving out of the dark than for those moving out of the light. This is a manifestation of the time scale of the lateral inhibitory transduction. At high speeds for steps coming out of the light the inhibitory

effect on the test ommatidium of the approaching on-transient lasts sufficiently long to sum with the excitatory transient when it arrives at the test ommatidium a few moments later; when the step approaches out of the dark, there is no anticipatory inhibition, and the on-transient is correspondingly greater in height.

A striking feature of the responses to high-speed stimuli is the presence of secondary maxima after the excitatory on-transients, in the full-eye and out-of-the-dark stimulus conditions. The separation between the principal excitatory peaks and these secondary maxima is constant when the response records are plotted on a constant "space scale" (Figs. 5 and 6). This implies that these secondary maxima are not features of the intrinsic impulse response of the test ommatidium, but rather represent genuine disinhibition of the test ommatidium by the strong inhibitory Mach band after the initial on-transient.

We have confirmed this description of the neural events responsible for the observed responses to the extent that variation of the model parameters corresponding to any particular physiological process produces the expected changes in the predicted response. It should also be possible to obtain more direct confirmation of this description by means of physiological manipulation of the *Limulus* eye. For example, many processes in the eye are known to be highly sensitive to the temperature of the preparation. It is also possible to alter the properties of the neural network pharmacologically (MacNichol and Benolken, 1956; Adolph, 1966, 1976; Adolph and Tuan, 1972). We have also observed variations in neural properties in "sick" *Limulus* specimens (Brodie et al., 1978*a*). In all such instances, variations in retinal physiology should produce analogous changes in both the empirical transfer function and the observed responses to moving stimuli, so that the former should continue to predict the latter.

We have suggested above that the truncated homogeneous network embodied in our simulated edge experiments is a useful model for the naturally occurring boundaries of real neural networks. The similarity between the observed responses near real and simulated edges in the *Limulus* retina suggests that this network may be an instance where such a model is valid. However, our data do not rule out various possibilities for the existence of modified network properties near the boundary of the *Limulus* retina. For example, our experiment on an ommatidium near the eye's actual boundary yielded a set of dynamical parameters within the normal range of our experience, with the notable exception of the total strength of lateral inhibition $[\mathbf{K}/(1 + \kappa)]$, which was roughly twice as large as we have ever measured for any ommatidium in the interior of a *Limulus* eye. This is consistent with unpublished observations of F. Dodge and E. Kaplan that the total inhibition converging on ommatidia at the bottom edge of the eye is equal to the total inhibition converging on ommatidia in the interior, despite the fact that these edge units lie entirely to one side of their inhibitory field. Such variation in the pattern of connectivity of the lateral plexus is presumably sufficiently gradual as to fit into our framework of a nearly homogeneous structure.

We observe that the neural organization at a boundary distinguishes the direction of motion across it. The response of a stimulus crossing a boundary from the interior portion is clearly different from the response to oppositely directed movement. Thus boundary neurons could act as primitive directional motion detectors.

We have thus demonstrated that the dynamic response of the *Limulus* retina at a simulated edge may be described quantitatively in terms of the same Hartline-Ratliff model as was developed to model the response of the full eye. This description is obtained by solving the

Hartline-Ratliff equations on the half-line, instead of the full line, by means of the Wiener-Hopf technique. The effect of the simulated edge configuration on the response of *Limulus* retinal neurons is significant. Responses measured near the physical boundary of the eye are qualitatively similar to those obtained at simulated edges in the interior. Such simple truncation of a homogeneous neural network may well serve as a model for edge effects at the boundaries of other neural networks.

APPENDIX

The result of monitoring the activity of an individual ommatidium is a list of firing times. This sequence may be transformed into a continuous function in more than one way. Thus, the mean individual rate, σ, is convenient for the representation of measured responses, while the population rate, r, is more useful for theoretical purposes, and for the measurement of transfer functions. In this Appendix, we consider some computational aspects of the relationship between these two functions, which go beyond the linear treatment in Brodie et al., 1978*a*.

Population Rate

Consider an ensemble or population of identical encoders, say N, in number. Then $r(t)$, the population rate, is defined so that in a small increment of time, δt, $Nr(t)\delta t$ gives the number of encoders that are firing. In the limit $N \uparrow \infty$ we expect $r(t)$ to become smooth. Next we define the instantaneous period $\tau(t)$ implicitly by:

$$\int_{t-\tau(t)}^{t} r(t)\,\mathrm{d}t = 1. \tag{A1}$$

τ may be interpreted as the elapsed time from the previous impulse to the present impulse.

Mean Individual Rate

If we denote the sequence of impulse times of an individual unit by

$$\ldots t_{n-1}, t_n, t_{n+1}, \ldots,$$

then the individual impulse rate is defined by

$$s(t) = \sum_n \frac{\mathcal{X}_n(t)}{t_{n+1} - t_n},$$

where the characteristic function, $\mathcal{X}_n(t)$, is unity for the interval $t_n < t \leq t_{n+1}$, and zero elsewhere. In each such interval, $s(t)$ has the constant value $1/(t_{n+1} - t_n)$, so that the piecewise constant function $s(t)$ has the appearance of a battlement. For M presentations of an identical stimulus, define the mean individual rate by

$$\sigma = \langle s \rangle = \frac{1}{M} \sum_{m=1}^{M} s_m(t),$$

where $s_m(t)$ is the individual rate for the mth presentation.[2]

To obtain the connection between $r(t)$ and $\sigma(t)$ we begin with the observation that in the limit of a large number, M, of repetitions, σ can be regarded as an ensemble average over the individual rates of the population.

To compute this average at some time t, we first note that only if t falls in the interval,

[2]The mean individual rate σ is the same function as was referred to as the "mean instantaneous rate" in Brodie et al., 1978*a*.

$$t' - \tau(t') < t \leq t', \tag{A2}$$

will an impulse fired at time t' contribute to the ensemble average $\sigma(t)$. In fact it gives rise to the individual rate

$$\frac{1}{t' - [t' - \tau(t')]} = \frac{1}{\tau(t')},$$

and the number of encoders in an interval dt' that have this property is given by:

$$N r(t')\, dt.$$

Next we denote by $(t, t + \theta)$ the time interval for which Eq. A2 holds. A little reflection shows that $\theta = \theta(t)$ is determined by

$$\theta = \tau(t + \theta). \tag{A3}$$

It therefore follows that the mean individual rate is given by

$$\sigma(t) = \int_t^{t+\theta(t)} \frac{r(t')\, dt'}{\tau(t')}. \tag{A4}$$

The equations A1, A3, and A4 constitute the set that relates σ and r, the mean indivudual and population rates, respectively.

We thank Professor Floyd Ratliff, who directed us to this problem, for his participation and encouragement in this project.

This work was supported in part by grants from the U.S. National Eye Institute, EY188, EY1428, and EY1472 and from the National Science Foundation, MC577-08598. L. Sirovich is grateful to the John Simon Guggenheim Memorial Foundation for fellowship support during the course of this work.

Received for publication 26 February 1979 and in revised form 10 August 1979.

REFERENCES

ADOLPH, A. R. 1966. Excitation and inhibition of electrical activity in the *Limulus* eye by neuropharmological agents. *In* Functional Organization of the Compound Eye. C. Bernhard, editor. Pergamon Press, Inc. Elmsford, N.Y. 465–482.

ADOLPH, A. R. 1973. Thermal sensitivity of lateral inhibition in *Limulus* eye. *J. Gen. Physiol.* **62**:392–406.

ADOLPH, A. R. 1976. Putative synaptic mechanisms of inhibition in *Limulus* lateral eye. *J. Gen. Physiol.* **67**:417–431.

ADOLPH, A. R., and F. J. Tuan. 1972. Serotinin and inhibition in *Limulus* lateral eye. *J. Gen. Physiol.* **60**:679–697.

BARLOW, R. B., JR. 1967. Inhibitory fields in the *Limulus* lateral eye. Ph.D. thesis. The Rockefeller University, New York.

BIEDERMAN-THORSON, M., and J. THORSON, 1971. Dynamics of excitation and inhibition in the light-adapted *Limulus* eye *in situ*. *J. Gen. Physiol.* **58**:1–19.

BRODIE, S. E. 1979. Temperature dependence of the dynamic response of the *Limulus* retina. *Vision Res.* **19**:91–94.

BRODIE, S. E., B. W. KNIGHT, and F. RATLIFF. 1978*a*. The response of the *Limulus* retina to moving stimuli. A prediction by Fourier synthesis. *J. Gen. Physiol.* **72**:129–166.

BRODIE, S. E., B. W. KNIGHT, and F. RATLIFF. 1978*b*. The spatiotemporal transfer function of the *Limulus* lateral eye. *J. Gen. Physiol.* **72**:167–202.

HARTLINE, H. K., and F. RATLIFF. 1957. Inhibitory interaction of receptor units in the eye of *Limulus*. *J. Gen. Physiol.* **40**:357–376.

JOHNSTON, D., and H. WACHTEL. 1976. Electrophysiological basis for the spatial dependence of the inhibitory coupling in the *Limulus* retina. *J. Gen. Physiol.* **67**:1–25.

KAPLAN, E. and R. B. BARLOW, JR. 1975. Properties of visual cells in the lateral eye of *Limulus in situ*. *J. Gen. Physiol.* **66**:303–326.

KNIGHT, B. W. 1972. Dynamics of encoding in a population of neurons. *J. Gen. Physiol.* **59**:734–766.
KNIGHT, B. W., S. F. BRODIE, and L. SIROVICH. 1979. On the treatment of nerve impulse data for comparison with experiment. *Proc. Natl. Acad. Sci. U.S.A.* In press.
MACNICHOL, E. F., JR., and R. BENOLKEN. 1956. Blocking effect of ethyl alcohol on inhibitory synapses in the eye of *Limulus. Science (Wash. D.C.)* **124**:681–682.
NOBLE, B. 1958. The Wiener-Hopf Technique. Pergamon Press, Inc., London. x & 246.
RATLIFF, F. 1965. Mach Bands: Quantitative Studies on Neural Networks in the Retina. Holden-Day, Inc., San Francisco. 365 pp.
RATLIFF, F., editor. 1974. Studies on Excitation and Inhibition in the Retina. The Rockefeller University Press, New York. 668 pp.
SIROVICH, L. 1980. Boundary effects in neural networks. *SIAM J. Appl. Math.* In press.
WIENER, N., and E. HOPF. 1931. Uber eine Klasse singulärer Integralgleichungen. Sitzungsberichte der Preussischen Akademie, Mathematisch-Physikalische Klasse, 1931. p. 696.